

# Resonant capture, counter-rotating disks, and polar rings

Scott Tremaine and Qingjuan Yu

*Princeton University Observatory, Peyton Hall, Princeton, NJ 08544-1001, USA*

Accepted ??? Received ??? in original form ???

## ABSTRACT

We suggest that polar rings and/or counter-rotating disks in flattened galaxies can be formed from stars captured at the Binney resonance, where the rate of precession of the angular momentum vector of a disk star equals the pattern speed of a triaxial halo. If the halo pattern speed is initially retrograde and slowly decays to zero, stars can be trapped as the Binney resonance sweeps past them, and levitated into polar orbits. If the halo pattern speed is initially retrograde and slowly changes to prograde, trapped stars can evolve from prograde to retrograde disk orbits. The stellar components of polar rings formed by this process should consist of two equal, counter-rotating star streams.

**Key words:** galaxies: formation – galaxies: general – galaxies: kinematics and dynamics

## 1 INTRODUCTION

This paper is motivated by the remarkable discovery (Rubin, Graham & Kenney 1992) that the otherwise normal E7/S0 galaxy NGC 4550 contains two stellar disks rotating in opposite directions. The two disks are similar in total luminosity and scale length and approximately coplanar (Rix et al. 1992); one is accompanied by an extended gas disk.

A second case of a counter-rotating disk is the Sab galaxy NGC 7217, in which 20–30% of the disk stars are on retrograde orbits, independent of radius (Merrifield & Kuijken 1994). Counter-rotating disks are rare: Kuijken, Fisher & Merrifield (1996) examined 28 S0 galaxies and found no counter-rotating components containing more than  $\sim 5\%$  of the total disk light. In contrast, roughly 20% of the gas disks in S0 galaxies counter-rotate (Bertola, Buson & Zeilinger 1992); however, these gas disks are generally much smaller than the accompanying stellar disks, so even if they form stars (as in NGC 3593, Bertola et al. 1996) they are unlikely to produce two stellar disks of similar size as in NGC 4550 or NGC 7217.

Several formation mechanisms for counter-rotating disks have been discussed. (i) A merger could add material on retrograde orbits to a pre-existing stellar disk, but mergers are likely to overheat the original disk even in favourable cases where the merging galaxy is gas-rich or its orbit lies in the original disk plane (Thakar & Ryden 1998). (ii) Hierarchical models of galaxy formation predict that the mean angular momentum of infalling gas varies substantially during the lifetime of a galaxy, so that early infall could produce a gas disk that later forms stars, while late infall subsequently brings in retrograde gas that forms stars in turn. This proposal does not explain why the scale lengths of counter-rotating disks are similar (Thakar & Ryden 1998), or why NGC 4550 satisfies the normal Tully-Fisher relation (Rix et al. 1992). (iii) Evans & Collett (1994) point out that box orbits in a triaxial potential can evolve into loop orbits if the potential slowly becomes more axisymmetric (an effect expected from late infall; Dubinski 1994). After this process stars will occupy both direct and retrograde loops—in precisely equal numbers if the triaxial potential is non-rotating—thereby naturally creating counter-rotating disks<sup>\*</sup>.

Polar-ring galaxies are early-type (usually S0) galaxies containing an outer ring of gas, dust and stars on orbits that are approximately circular and nearly perpendicular to the symmetry plane of the galaxy. At least 0.5% of S0 galaxies have polar rings, although this is probably an underestimate because of orientation-dependent selection effects (Whitmore et al. 1990). The catalog by Whitmore et al. lists only six kinematically confirmed polar-ring galaxies but many more candidates without kinematic data. Like counter-rotating disks, polar rings are usually assumed to form from the merger of a companion galaxy or late gas infall (e.g. Katz & Rix 1992, Bekki 1998); if the gravitational potential of the primary galaxy is triaxial then there

<sup>\*</sup> The dynamical stability of counter-rotating disks is discussed by Sellwood & Merritt (1994).

is a range of initial conditions from which dissipative material will settle into a polar orbit perpendicular to the long axis (Steiman-Cameron & Durisen 1984; Thomas, Vine & Pearce 1994).

In this paper we describe a novel way to form counter-rotating disks and/or polar rings. The inclinations of disk-star orbits can be excited by resonant coupling to a triaxial halo potential. The location of the relevant resonances is determined by the vertical and azimuthal frequencies,  $\Omega_2$  and  $\Omega_3$  (see §2), and the pattern speed of the halo,  $\Omega_p$ . In particular, Binney (1978, 1981) has stressed the importance of the resonance at

$$\Omega_3 - \Omega_2 = \Omega_p, \quad (1)$$

which we call the Binney resonance. The Binney resonance occurs when the pattern speed matches the rate of precession of the angular momentum vector or node,  $\dot{\omega} = \Omega_3 - \Omega_2$ . For low-inclination orbits in oblate potentials,  $\Omega_2 > \Omega_3$ , so the Binney resonance occurs for retrograde pattern speed.

We suppose that the disk is embedded in a triaxial halo that initially rotates with a retrograde pattern speed  $\Omega_{pi} < 0$ . The pattern speed is expected to change slowly as the halo acquires dark matter by infall; we assume that the pattern speed increases, reaching a final value  $\Omega_{pf} \geq 0$ . If  $\Omega_p$  changes sufficiently slowly, stars with small initial inclinations  $i_0$  are trapped in the Binney resonance as  $\Omega_p$  sweeps past  $\Omega_3 - \Omega_2$ . As  $\Omega_p$  increases further, the orbits of the trapped stars are levitated (Sridhar & Touma 1996) to higher inclination while remaining nearly circular, becoming polar orbits as  $\Omega_p$  crosses zero. Thus if  $|\Omega_p|$  gradually decays to zero, an outer polar ring is formed from disk stars with  $\Omega_2 - \Omega_3 < |\Omega_{pi}|$ . If  $\Omega_p$  crosses zero to positive values, the trapped stars evolve onto retrograde orbits, until they are eventually released from the Binney resonance when  $\Omega_p$  sweeps through  $-\Omega_2 + \Omega_3 > 0$ . The inclinations after release are near  $\pi - i_0$ , so the flipped stars form a counter-rotating disk with the same thickness as the initial disk.

A close cousin of this process was already discussed by Heisler, Merritt & Schwarzschild (1982; see also van Albada, Kotanyi & Schwarzschild 1982). They recognized that a sequence of ‘‘anomalous’’ inclined orbits bifurcated from the closed short-axis loop orbits at the Binney resonance in a rotating triaxial potential, and speculated that gas might evolve onto the anomalous orbits as a result of dissipation. However, they focused on a sequence of orbits of decreasing energy at fixed pattern speed, which terminates in a short-axis orbit that cannot be occupied by collisional material. In contrast, we examine the behavior of dissipationless material in a system with time-varying pattern speed. Our mechanism is also related to the levitation process discussed by Sridhar & Touma (1996), who focus on a different resonance as a means of forming a thick disk.

In §2 we describe the classification of resonances in nearly axisymmetric potentials and justify our focus on the Binney resonance. In §3 we investigate capture and release of stars at the Binney resonance using a simplified dynamical model. §4 describes the results of numerical integrations, and §5 contains a discussion.

## 2 RESONANCE CLASSIFICATION

To determine the most promising sites for resonant capture, we first consider integrable motion in an axisymmetric potential. We define action-angle variables  $(\mathbf{I}, \mathbf{w})$ , such that  $H_0 = H_0(\mathbf{I})$  is the axisymmetric Hamiltonian and the trajectory of a particle is given by

$$\mathbf{I} = \text{const}, \quad \mathbf{w} = \text{const} + \boldsymbol{\Omega}t, \quad (2)$$

where

$$\boldsymbol{\Omega}(\mathbf{I}) = \frac{\partial H_0}{\partial \mathbf{I}}. \quad (3)$$

The actions in a spherical potential can be chosen as follows:  $I_1$  is the radial action, which is zero for circular orbits;  $I_2$  is the vertical or latitudinal action, which is zero for prograde equatorial orbits and in general is equal to  $J - J_z$ , where  $J$  is the total angular momentum and  $J_z$  its  $z$ -component;  $I_3$  is the azimuthal action, which is equal to  $J_z$ . Note that  $I_1 \geq 0$ ,  $I_2 \geq 0$ ,  $I_3 \leq \frac{1}{2}I_2$ .

The geometrical interpretation of these actions remains similar for integrable axisymmetric Hamiltonians (de Zeeuw 1985); in particular,  $I_3$  is still equal to  $J_z$ , prograde equatorial orbits still have  $I_2 = 0$ , and the analogs of circular orbits ( $I_1 = 0$ ) are shell orbits, which occupy a two-dimensional axisymmetric surface of zero thickness.

Now we add a weak, non-axisymmetric perturbing potential of the form

$$U_1(\mathbf{r}, t) = A(r, \theta) \cos\{m[\phi - \phi_p(t)]\}, \quad (4)$$

where  $m \neq 0$  is a positive integer and  $\dot{\phi}_p \equiv \Omega_p$  is the pattern speed. In action-angle variables this potential can be written as (e.g. Tremaine & Weinberg 1984)

$$U_1(\mathbf{I}, \mathbf{w}, t) = \sum_{\mathbf{k}} A_{\mathbf{k}}(\mathbf{I}) \cos[\mathbf{k} \cdot \mathbf{w} - m\phi_p(t)] \quad (5)$$

where  $\mathbf{k}$  is an integer triple, with  $k_3 = m$ . Terms in the perturbing potential (5) with  $k_3 = 0$  conserve the azimuthal action  $I_3 = J_z$ ; terms with  $k_1 = 0$  conserve the radial action  $I_1$ ; and terms with  $k_2 = 0$  conserve the vertical action  $I_2 = J - J_z$ . When  $I_1 = 0$  the radial angle  $w_1$  is undefined, so  $A_{\mathbf{k}}(I_1 = 0)$  must vanish for  $k_1 \neq 0$ ; more generally  $A_{\mathbf{k}} \rightarrow I_1^{|k_1|/2}$  as  $I_1 \rightarrow 0$ . Similarly  $A_{\mathbf{k}} \rightarrow I_2^{|k_2|/2}$  as  $I_2 \rightarrow 0$  (in celestial mechanics these constraints are called the d'Alembert characteristic). We shall assume that the perturbing potential is symmetric around the equatorial plane, which requires that  $A_{\mathbf{k}} = 0$  unless  $k_2$  is even.

We are interested in the resonant excitation of inclination in low-inclination, near-circular disk orbits. Resonance occurs when the rate of change of the resonant angle  $\mathbf{k} \cdot \mathbf{w} - m\phi_p(t)$  is zero, yielding the resonance condition

$$\mathbf{k} \cdot \boldsymbol{\Omega} = m\Omega_p. \quad (6)$$

Since  $A_{\mathbf{k}} \rightarrow 0$  as  $I_1 \rightarrow 0$  when  $k_1 \neq 0$ , the strongest inclination excitation for near-circular orbits comes from terms with  $k_1 = 0$ . We shall also focus on terms with  $k_3 = m = 2$ , since barlike and triaxial perturbations are the strongest non-axisymmetric features in galaxies. Since  $A_{\mathbf{k}} \propto I_2^{|k_2|/2}$ , near-equatorial orbits are most strongly affected by terms with  $k_2 = 0, \pm 2$  (recall that  $k_2$  must be even); however, resonances with  $k_2 = 0$  cannot excite inclination (for these resonances  $w_2$  is ignorable, so the vertical action  $I_2$  is conserved), so we restrict our attention to  $k_2 = \pm 2$ . For the triples  $\mathbf{k} = (0, \pm 2, 2)$  the resonance condition (6) is

$$\pm \Omega_2 + \Omega_3 = \Omega_p. \quad (7)$$

In potentials that are not highly flattened, the vertical and azimuthal frequencies are similar,  $\Omega_2 \sim \Omega_3$ . If the pattern speed is slow,  $|\Omega_p| < \Omega_{2,3}$  (as would be expected for the perturbation from a triaxial halo) resonance is therefore more likely to occur for  $k_2 = -2$  than for  $k_2 = 2$ . Thus we are led naturally to the Binney resonance  $\mathbf{k} = (0, -2, 2)$  (eq. 1).

At the Binney resonance  $I_1$  is adiabatically invariant because the perturbations with  $k_1 \neq 0$  are rapidly varying. Moreover  $w_2$  and  $w_3$  appear in the potential only in the combination  $2(w_3 - w_2)$ , so  $I_2 + I_3$  is conserved. In nearly spherical potentials  $I_2 + I_3 \simeq J$ , so the total angular momentum is approximately conserved. In other words the resonance affects only the inclination of the orbit, and not its total angular momentum or eccentricity. In effect, the evolution of a circular orbit near the Binney resonance is that of a rigid spinning hoop with the same radius and angular momentum, an analogy that we shall pursue in the next section.

### 3 A SIMPLIFIED MODEL FOR RESONANCE CAPTURE

We consider motion in a rotating, triaxial potential of the form

$$U(\mathbf{r}, t) = \Phi \left( \tilde{x}^2 + \frac{\tilde{y}^2}{p^2} + \frac{z^2}{q^2} \right); \quad (8)$$

here the rotating coordinates  $(\tilde{x}, \tilde{y})$  are related to the inertial coordinates  $(x, y)$  by

$$x + iy = (\tilde{x} + i\tilde{y}) \exp(i\phi_p), \quad \frac{d\phi_p}{dt} = \Omega_p(t), \quad (9)$$

where  $\Omega_p$  is the pattern speed. We assume that the  $x$ -axis is the long axis, so  $0 < p, q \leq 1$ , and that the symmetry plane of the disk is the  $x$ - $y$  plane. Since loop orbits around the intermediate axis are unstable, the  $z$ -axis must be the short axis, so  $q < p$ . Thus

$$0 < q < p \leq 1. \quad (10)$$

We assume that the axis ratios are not too far from unity—typically we choose  $q = 0.8$ ,  $p = 0.9$ —so we can expand the potential as

$$U(\mathbf{r}, t) = \Phi(r^2) + \frac{V^2}{2r^2} [(p^{-2} - 1)\tilde{y}^2 + (q^{-2} - 1)z^2]; \quad (11)$$

here we have replaced  $d\Phi/dr^2$  by  $\frac{1}{2}V^2/r^2$  where  $V(r)$  is the circular speed at radius  $r$ .

For simplicity we assume that the time variation of the pattern speed is given by

$$\Omega_p(t) = \dot{\Omega}_p t, \quad (12)$$

where  $\dot{\Omega}_p$  is a constant.

Since we are interested in nearly circular orbits, we replace the particle by a circular hoop of radius  $r$ ; the angular momentum of the hoop is a constant  $J$  and its orientation is specified by the canonical momentum-coordinate pair  $(J_z, \omega)$ , where  $J_z = J \cos i$  is the  $z$ -component of the angular momentum,  $i$  is the inclination, and  $\omega$  is the longitude of the ascending node. The Hamiltonian of the hoop is  $H(J_z, \omega, t) = \langle U(\mathbf{r}, t) \rangle$ , where  $\langle \cdot \rangle$  denotes an average over the hoop. Neglecting unimportant

constants we have

$$\begin{aligned} H(J_z, \omega, t) &= \frac{V^2}{4} \{ (p^{-2} - 1) [\sin^2(\omega - \phi_p) + \cos^2 i \cos^2(\omega - \phi_p)] + (q^{-2} - 1) \sin^2 i \} \\ &= -\frac{V^2}{8} \left[ (2q^{-2} - p^{-2} - 1) \frac{J_z^2}{J^2} + (p^{-2} - 1) \left( 1 - \frac{J_z^2}{J^2} \right) \cos 2(\omega - \phi_p) \right]. \end{aligned} \quad (13)$$

Throughout this analysis we can consider  $V$  to be constant, since the radius of the hoop is fixed.

We now convert to new canonical variables  $(W, w) = (J_z/J, \omega - \phi_p)$  and a dimensionless time  $s = t/(J\beta)$ , where  $\beta$  is a constant to be chosen below. Using equation (12) for the time-dependence of the pattern speed, the new Hamiltonian is found to be

$$\begin{aligned} H(W, w, s) &= -\frac{\beta V^2}{8} (2q^{-2} - p^{-2} - 1) W^2 \\ &\quad - \frac{\beta V^2}{8} (p^{-2} - 1) (1 - W^2) \cos 2w - (\beta^2 J^2 \dot{\Omega}_p) W s. \end{aligned} \quad (14)$$

We choose the timescale parameter  $\beta$  so that the coefficient of  $W^2$  is  $-\frac{1}{2}$ ; thus

$$H(W, w, s) = -\frac{1}{2} W^2 - \alpha (1 - W^2) \cos 2w - \gamma W s, \quad (15)$$

where

$$\begin{aligned} \alpha &= \frac{p^{-2} - 1}{2(2q^{-2} - p^{-2} - 1)}, \\ \beta &= \frac{4}{V^2(2q^{-2} - p^{-2} - 1)}, \\ \gamma &= \frac{16r^2 \dot{\Omega}_p}{V^2(2q^{-2} - p^{-2} - 1)^2}; \end{aligned} \quad (16)$$

here we have replaced  $J$  by  $rV$ , its value when  $p$  and  $q$  are near unity. The constraints (10) imply that

$$0 < \alpha < \frac{1}{2}, \quad \beta > 0, \quad (17)$$

and  $\text{sgn}(\gamma) = \text{sgn}(\dot{\Omega}_p)$ ; for the axis ratios  $q = 0.8$ ,  $p = 0.9$ , we have  $\alpha = 0.1317$ .

The Hamiltonian (15) depends on two parameters:  $\alpha$ , which determines the strength of the non-axisymmetric potential, and  $\gamma$ , which determines the speed of the resonance passage. In the limit where the potential is nearly spherical,  $1 - p, 1 - q = \mathcal{O}(\epsilon) \ll 1$ , we have  $\alpha = \mathcal{O}(1)$ ,  $\beta = \mathcal{O}(\epsilon^{-1})$ ,  $\gamma = \mathcal{O}(\dot{\Omega}_p \epsilon^{-2})$ . The phase space is a sphere of unit radius with a simple physical interpretation: the angular-momentum vector  $\mathbf{J}$  has azimuth  $w + \phi_p - \frac{1}{2}\pi$  and colatitude  $i = \cos^{-1} W$ .

We are interested in the case where the pattern speed changes slowly,  $|\dot{\Omega}_p| \ll \epsilon^2$  or  $|\gamma| \ll 1$ . In this case, over short times the trajectory closely follows a level curve of the Hamiltonian for fixed  $s$ ,  $H(W, w, s) = h(s)$  (the ‘‘guiding trajectory’’). The nature of the guiding trajectories depends on the topology of the level surfaces of  $H$ . In describing this topology we restrict ourselves to  $0 < \alpha < \frac{1}{2}$ , as required by equation (17); we may then distinguish the following stages (Figure 1):

(a)  $\gamma s < -2\alpha - 1$ : There are stable equilibrium points at  $W = 1$  (north pole) and  $W = -1$  (south pole); the angle  $w$  circulates for all orbits.

(b)  $-2\alpha - 1 < \gamma s < 2\alpha - 1$ : There is a stable equilibrium point at the south pole, and an unstable equilibrium or saddle point at the north pole. There are also stable equilibria at  $w = \pm \frac{1}{2}\pi$ ,  $W = -\gamma s / (1 + 2\alpha)$ . The separatrix orbit passing through the north pole has energy  $h_{\text{sep}} = -\frac{1}{2} - \gamma s$ , and divides circulating orbits with  $h < h_{\text{sep}}$  from librating orbits with  $h > h_{\text{sep}}$ .

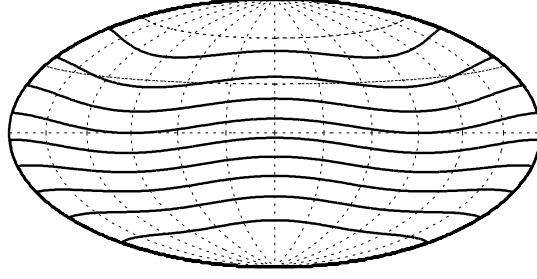
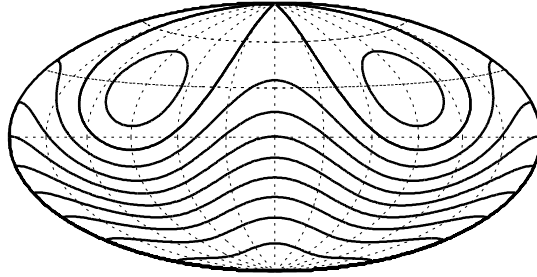
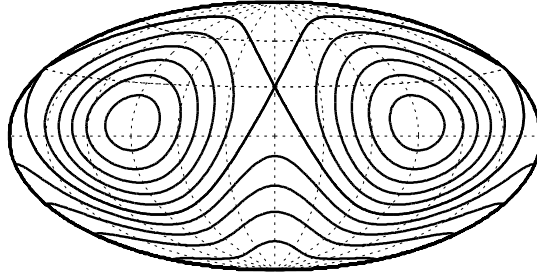
(c)  $2\alpha - 1 < \gamma s < -2\alpha + 1$ : There are stable equilibrium points at both poles, as well as stable equilibria at  $w = \pm \frac{1}{2}\pi$ ,  $W = -\gamma s / (1 + 2\alpha)$ . In addition there are unstable equilibria at  $w = \{0, \pi\}$ ,  $W = -\gamma s / (1 - 2\alpha)$ . The separatrix orbit passing through the unstable equilibria has energy  $h_{\text{sep}} = \frac{1}{2}(\gamma s)^2 / (1 - 2\alpha) - \alpha$ , and divides circulating orbits with  $h < h_{\text{sep}}$  from librating orbits with  $h > h_{\text{sep}}$ .

(d)  $-2\alpha + 1 < \gamma s < 2\alpha + 1$ : This is identical to stage (b) after the transformation  $\gamma s \rightarrow -\gamma s$ ,  $W \rightarrow -W$ . There are stable and unstable equilibria at the north and south poles respectively, and stable equilibria at  $w = \pm \frac{1}{2}\pi$ ,  $W = -\gamma s / (1 + 2\alpha)$ .

(e)  $2\alpha + 1 < \gamma s$ : This is identical to stage (a) after the transformation  $\gamma s \rightarrow -\gamma s$ ,  $W \rightarrow -W$ : there are stable equilibria at  $W = \pm 1$  and  $w$  circulates for all orbits.

Adiabatic invariance ensures that over long times the guiding trajectory evolves so as to preserve the action, which is  $(2\pi)^{-1}$  times the area on the phase-space sphere enclosed by the guiding trajectory (e.g Peale 1976, Henrard 1982, Borderies & Goldreich 1984, Engels & Henrard 1994).

Let us follow the evolution of the orbit for the case  $\gamma > 0$ , corresponding to a pattern speed that is initially negative (retrograde) but increasing. At large negative time,  $\gamma s \ll -1$ , the Hamiltonian (15) is dominated by the term  $-\gamma W s$  and the guiding trajectory is  $W = W_0 = \text{constant}$ , where  $W_0 = \cos i_0$  and  $i_0$  is the initial inclination. The initial action is  $(2\pi)^{-1}$  times the area of the north polar cap on the phase-space sphere that is enclosed by the initial trajectory, and is equal to  $1 - W_0$ .

(a)  $\alpha=0.3$ ,  $\gamma s=-4.0$ 

 (b)  $\alpha=0.3$ ,  $\gamma s=-0.7$ 

 (c)  $\alpha=0.3$ ,  $\gamma s=-0.2$ 


**Figure 1.** Topology of the level surfaces of the Hamiltonian (15), for  $\alpha < \frac{1}{2}$ . The plots show equal-area Aitoff projections of the sphere with longitude  $w$  and colatitude  $i = \cos^{-1} W$ , where  $i$  is the inclination and  $w \in [-\pi, \pi]$  is the longitude of the ascending node in the frame rotating at the pattern speed  $\Omega_p$ . The plots show only stages (a)–(c); stages (d) and (e) are upside-down versions of (b) and (a) respectively.

As the time  $s$  increases, the topology of the Hamiltonian eventually changes from stage (a) to stage (b). In the initial phases of stage (b), the guiding trajectory continues to circulate, despite the growing libration zones defined by the separatrix orbit through the north pole. Eventually the area occupied by the libration zones grows to  $2\pi(1 - W_0)$ , so the action can no longer be conserved if the orbit continues to circulate. At this point the guiding trajectory crosses the separatrix and is captured into one of the two libration zones.

The area occupied by the libration zones in stage (b) can be evaluated analytically,

$$A(\gamma s) = \frac{4\gamma s}{(1 - 4\alpha^2)^{1/2}} \cos^{-1} \frac{1 + \gamma s - 4\alpha^2}{2\alpha\gamma s} + 4 \cos^{-1} \frac{-1 - \gamma s}{2\alpha}, \quad -2\alpha - 1 \leq \gamma s \leq 2\alpha - 1. \quad (18)$$

As the time  $s$  increases,  $A(\gamma s)$  increases from zero at the onset of stage (b) to  $A_{\max}$  at the onset of stage (c), where

$$A_{\max} = A(2\alpha - 1) = 4\pi \left[ 1 - \left( \frac{1 - 2\alpha}{1 + 2\alpha} \right)^{1/2} \right]. \quad (19)$$

Capture into libration occurs when  $A = 2\pi(1 - W_0)$  and is certain if  $A_{\max} > 2\pi(1 - W_0)$ ; in other words capture is certain if

$$\cos i_0 > 2 \left( \frac{1 - 2\alpha}{1 + 2\alpha} \right)^{1/2} - 1. \quad (20)$$

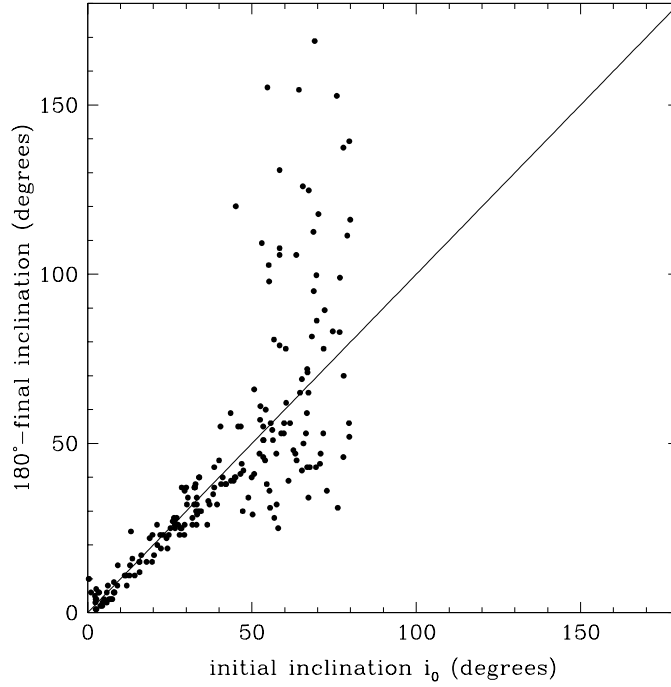


**Figure 2.** Initial inclination  $i_0$  versus final inclination for initially circular orbits with radius  $r = 1$  in the triaxial potential defined by equation (22). The evolution of the pattern speed is given by equation (23), with  $\Omega_{pf} = -\Omega_{pi} = 0.4$  and  $\tau = 5000$ . For  $i_0 \lesssim 50^\circ$ , the final inclination is  $\simeq 180^\circ - i_0$ .

For our nominal value  $\alpha = 0.1317$ , capture is certain if the initial inclination  $i_0 < 58.2^\circ$ . For larger inclinations, capture is probabilistic because the guiding trajectory crosses the separatrix orbit during stage (c), where transition to either libration or circulation can occur. In this case the capture probability can be computed using methods described by Henrard (1982).

The captured orbits remain librating through stage (c) and in the initial phases of stage (d). Eventually they re-cross the separatrix into circulation; by symmetry their final inclination is just  $i_f = \pi - i_0$ . In other words, a disk of stars in direct rotation is flipped into a disk with the same radial profile and thickness but in retrograde rotation. This mechanism operates if (i) The initial pattern speed  $\Omega_{pi}$  corresponds to stage (a) and the final pattern speed  $\Omega_{pf}$  to stage (e); this requires

$$\Omega_{pi} < -\frac{V}{2r}(q^{-2} - 1), \quad \Omega_{pf} > \frac{V}{2r}(q^{-2} - 1). \quad (21)$$

This condition can be restated in terms of  $\dot{\omega} = \Omega_3 - \Omega_2$ , the nodal precession rate for low-inclination orbits, as  $\Omega_{pi} < \dot{\omega}$ ,  $\Omega_{pf} > -\dot{\omega}$ . (ii) The pattern speed changes slowly enough that the action is adiabatically invariant except near the separatrix. (iii) The initial inclination of the disk stars is sufficiently small (eq. 20).

Another interesting outcome occurs if the pattern speed is initially retrograde and slowly decays to zero. In this case the stars will be trapped in polar orbits (stage (c) with  $s = 0$ ); the trapping process populates the two separatrices equally, so the resulting polar ring will itself form a counter-rotating disk, perpendicular to the long axis of the triaxial potential.

#### 4 NUMERICAL RESULTS

We have followed the evolution of test-particle orbits in a rotating triaxial potential of the form

$$U(\mathbf{r}, t) = \frac{1}{2}V^2 \log \left( \tilde{x}^2 + \frac{\tilde{y}^2}{p^2} + \frac{z^2}{q^2} \right), \quad (22)$$

where  $V$  is a constant and  $\tilde{x}$  and  $\tilde{y}$  are defined by equation (9). We take axis ratios  $q = 0.8$ ,  $p = 0.9$  and set  $V = 1$ . The particle is initially on a circular orbit with radius  $r = 1$ . The pattern speed is assumed to vary as

$$\Omega_p(t) = \Omega_{pi} + (\Omega_{pi} - \Omega_{pf}) (e^{-t/\tau} - 1), \quad (23)$$

and the orbits are followed from  $t = 0$  to  $t = 4\tau$ . With these parameters the star can undergo resonant capture and release if (eq. 21)

$$\Omega_{pi} < -0.281, \quad \Omega_{pf} > 0.281. \quad (24)$$

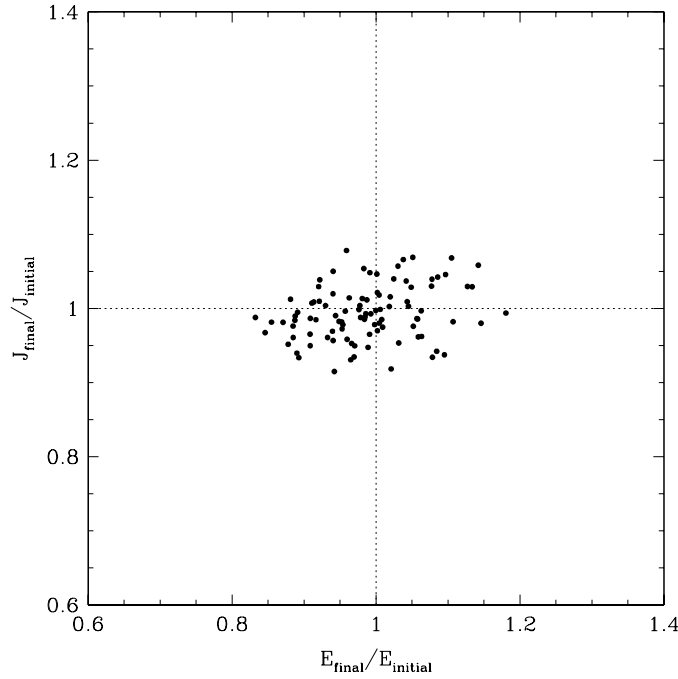


**Figure 3.** Final energy and angular momentum for the flipped particles in Figure 2 ( $i_0 < 40^\circ$ ). The initial energy and angular momentum are shown by dashed lines. The changes in both quantities are small, confirming that the size and shape of the orbit are not changed by the Binney resonance.

To illustrate resonant capture and release in the adiabatic limit, we have numerically integrated the orbits of 200 test particles with random orbital phases and nodes, varying the pattern speed according to the parameters  $\Omega_{pi} = -0.4$ ,  $\Omega_{pf} = +0.4$ ,  $\tau = 5000$ . The results are shown in Figure 2: stars with initial inclination  $i_0 \lesssim 50^\circ$  are flipped to inclination  $\sim 180^\circ - i_0$ , while for  $i_0 \gtrsim 50\text{--}60^\circ$  the final inclination exhibits a wide spread. These results are consistent with the conclusion from §3 that resonant capture was certain for these parameters if  $i_0 < 58.2^\circ$ . Figure 3 shows that the fractional changes in total angular momentum and energy of the flipped particles are  $\lesssim 0.1$ , confirming that capture in the Binney resonance changes only the inclination of the particle orbits, not their size or shape.

To investigate the validity of the adiabatic approximation, we have integrated 200 test particles with  $\tau$  varying from 100 to 2000, and initial inclinations distributed as  $n(i_0)di_0 \propto i_0 di_0 \exp(-\frac{1}{2}i_0^2/\sigma^2)$ , with  $\sigma = 5^\circ$ . The distribution of final inclinations shown in Figure 4 shows that most stars are captured when  $\tau \gtrsim 300$ ; in physical units this corresponds to  $\tau \gtrsim 7.5 \text{ Gyr}(r/5 \text{ kpc})(200 \text{ km s}^{-1}/V)$ .

We have also investigated the case where the pattern speed is initially retrograde and slowly decays to zero. Figure 5 shows the distribution of final inclinations as a function of the timescale  $\tau$ , for  $\Omega_{pi} = -0.4$ ,  $\Omega_{pf} = 0$ . The initial inclination range was  $i_0 = 0\text{--}10^\circ$ . For  $\tau \gtrsim 100$  most of the particles are trapped in orbits with inclination near  $90^\circ$ , thus forming a polar ring. The angular-momentum vectors are aligned with the long axis of the potential, with equal numbers of stars having  $J_x > 0$  and  $J_x < 0$ . Thus the polar ring is itself a counter-rotating disk.

Finally, we have examined whether resonance capture can occur in disk galaxies, by integrating test-particle orbits in a non-axisymmetric Miyamoto-Nagai potential

$$\Phi(R, z) = -\frac{GM}{(\tilde{x}^2 + \tilde{y}^2/p^2 + (a + (b^2 + z^2)^{1/2})^2)^{1/2}}, \quad (25)$$

where  $\tilde{x}$  and  $\tilde{y}$  are defined in equation (9) and  $a = 0.5$ ,  $b = 0.1$ . The particles are initially in circular orbits of unit radius, and the pattern speed varies according to (23) with  $\Omega_{pi} = -2$ ,  $\Omega_{pf} = 2$ . We find that for initial inclination  $i_0 \lesssim 6^\circ$ , most particles are captured and flipped into retrograde orbits with inclination  $180^\circ - i_0$ . The maximum inclination of the flipped orbits depends on the parameter  $b$ , which controls the thickness of the disk mass distribution; for  $b = 0.2$  most particles are flipped if  $i_0 \lesssim 15\text{--}20^\circ$ .

## 5 DISCUSSION

In rotating triaxial potentials with time-varying pattern speed, stars on short-axis loop orbits can be captured at the Binney resonance, where the pattern speed matches the precession rate  $\dot{\omega}$  of the angular momentum vector. As the pattern speed

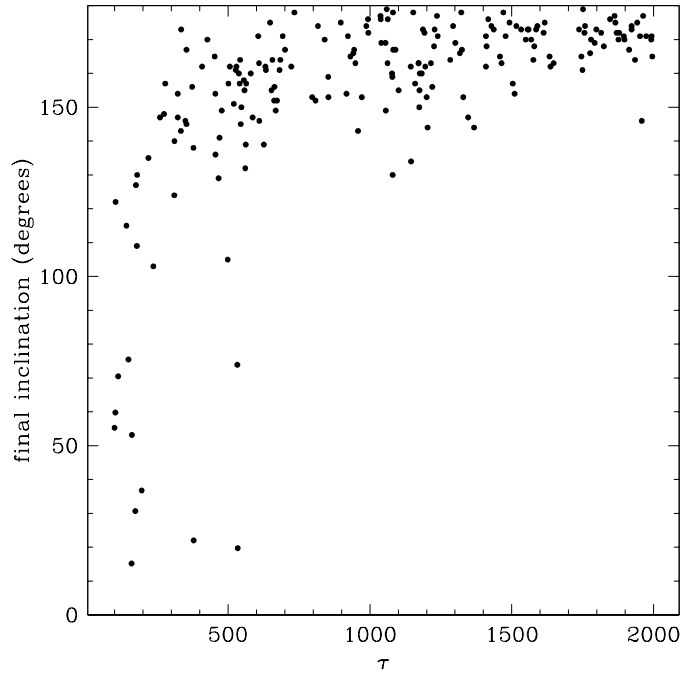


**Figure 4.** (top) Final inclination for initially circular orbits with radius  $r = 1$  in the triaxial potential defined by equations (22) and (23), with  $\Omega_{pi} = -0.4$ ,  $\Omega_{pf} = 0.4$ , and  $\tau$  varying from 100 to 2000. The initial inclinations are distributed as  $dN \propto i_0 \exp(-\frac{1}{2}i_0^2/\sigma^2)di_0$ , where  $\sigma = 5^\circ$ . The final inclinations are clustered near  $180^\circ$  for  $\tau \gtrsim 300$ .

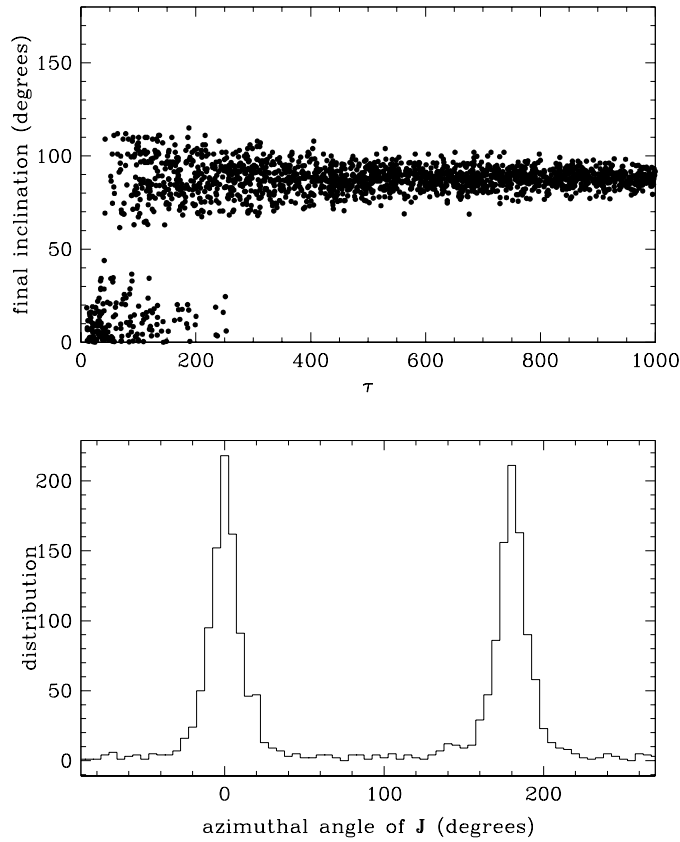


**Figure 5.** (top) Final inclination for initially circular orbits with radius  $r = 1$  in the triaxial potential defined by equations (22) and (23), with  $\Omega_{pi} = -0.4$ ,  $\Omega_{pf} = 0$ , and  $\tau$  varying from 10 to  $10^3$ . The final inclinations are clustered near  $90^\circ$ , so the captured stars form a polar ring. (bottom) Distribution of the azimuthal angle of the final angular momentum vector in the rotating frame. The angular momentum vectors are centered on the long or  $x$ -axis of the potential, with equal numbers of stars rotating in opposite directions.



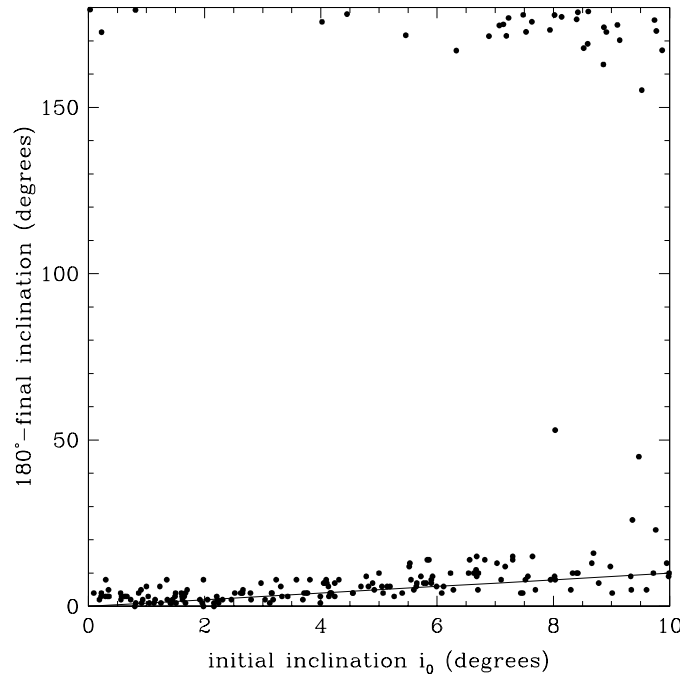


**Figure 6.** Initial inclination  $i_0$  versus final inclination for initially circular orbits with radius  $r = 1$  in the Miyamoto-Nagai potential (25) with  $a = 0.5$ ,  $b = 0.1$ . The evolution of the pattern speed is given by equation (23), with  $\Omega_{pf} = -\Omega_{pi} = 2$  and  $\tau = 2000$ . For  $i_0 \lesssim 6^\circ$ , the final orbits are retrograde and equatorial.

continues to change, captured stars will be carried to high inclinations without large changes in energy or total angular momentum.

Binney’s (1981) original discussion focused on the linear response of stars close to the resonance when the pattern speed was fixed. In contrast, by exploiting the theory of slow (adiabatic) resonant capture (Peale 1976; Henrard 1982; Borderies & Goldreich 1984; Engels & Henrard 1994), we can follow the nonlinear orbital evolution so long as the variation in pattern speed is slow enough.

It is striking that slow resonant capture and subsequent inclination growth is certain for stars with inclination  $i \simeq 0$ , no matter how weak the triaxial potential may be, even though  $i = 0$  is a formal solution of the equations of motion for the model Hamiltonian (13) for all time. The resolution of this apparent paradox is that (i) a Mathieu-type linear inclination instability is always present when the star is sufficiently close to resonance (Binney 1981); (ii) as the strength of the non-axisymmetry approaches zero, the drift rate of the pattern speed must also approach zero in order that the adiabatic approximation is valid.

If the final pattern speed of the triaxial potential is near zero, stars captured into the Binney resonance will form a polar ring of long-axis loop orbits. This model explains naturally why polar rings do not extend to the center of the galaxy: only stars whose initial precession rate  $|\dot{\omega}|$  is less than the initial pattern speed  $|\Omega_{pi}|$  can be captured. The stellar component of polar rings formed by this mechanism should exhibit two equal, counter-rotating star stream, a testable prediction.

If the final pattern speed is positive and larger than the precession rate of the angular momentum vector,  $\Omega_{pf} > |\dot{\omega}|$ , stars captured into the resonance with initial inclination  $i_0$  will be flipped onto retrograde orbits and then released with final inclination  $\pi - i_0$ . In disk potentials only the low-inclination fraction of the disk orbits are captured and flipped (Fig. 6), so both the direct and retrograde disk can be composed of pre-existing stars. For mildly triaxial potentials, capture is certain for orbits with small or moderate inclinations; in this case we must rely on subsequent star formation to re-form the parent disk. This model explains naturally why the two components of the counter-rotating disks in NGC 4550 and NGC 7217 have similar scale lengths. It does not explain why the two components in NGC 4550 have similar luminosity but then the two components in NGC 7217 do not, and in any case there are strong selection effects that favor the discovery of counter-rotating disks with similar luminosity.

A concern with this model is whether the required timescale for variation of the pattern speed is unrealistically slow. The time unit in our simulations is  $2.4 \times 10^7 \text{ yr}(r/5 \text{ kpc})(200 \text{ km s}^{-1}/V)$ , so timescales  $\tau \gtrsim 400$  may exceed  $10^{10} \text{ yr}$ , the natural timescale for variations in halo pattern speed. This should be compared with  $\tau \gtrsim 300$  required to flip orbits in the triaxial potential (Fig. 4) and  $\tau \gtrsim 1000$  to flip orbits in the Miyamoto-Nagai disk (Fig. 6). On the other hand we have used over-simplified model potentials and have not explored parameter space systematically.

Another issue is whether gravitational noise due to molecular clouds or spiral arms degrades the effectiveness of resonant capture, although this is not a problem for the majority of polar rings that are found in S0 galaxies.

An unresolved question is whether significant quantities of gas can be captured into the Binney resonance. The orbits of particles in the two libration zones around  $w = \pm\frac{1}{2}\pi$  intersect, so gas clouds in the two zones will collide at high speed, leading to rapid energy dissipation. There are thus two possibilities: either no gas is captured, or all of the gas is captured into one of the libration zones, leaving the other vacant. Numerical simulations are the best way to determine which of these two outcomes is more realistic<sup>†</sup>.

This research was supported in part by NSF Grant AST-9900316 and NASA Grant NAG5-7066.

## REFERENCES

- Bekki K. 1998, ApJ 499, 635  
 Bertola F., Buson L. M., & Zeilinger W. W. 1992, ApJ 401, L79  
 Bertola F., et al. 1996, ApJ 458, L67  
 Binney J. 1978, MNRAS 183, 779  
 Binney J. 1981, MNRAS 196, 455  
 Borderies N., & Goldreich P. 1984, Cel. Mech. 32, 127  
 Christodoulou D. M., Katz N., Rix H.-W., & Habe A. 1992, ApJ 395, 113  
 de Zeeuw T. 1985, MNRAS 216, 273  
 Dubinski J. 1994, ApJ 431, 617  
 Engels J. R., & Henrard, J. 1994, Cel. Mech. Dyn. Astr. 58, 215  
 Evans N. W., & Collett J. L. 1994, ApJ 420, L67  
 Habe A., & Ikeuchi S. 1985, ApJ 289, 540  
 Heisler J., Merritt D., & Schwarzschild M. 1982, ApJ 258, 490  
 Henrard J. 1982, Cel. Mech. 27, 3  
 Katz N., & Rix, H.-W. 1992, ApJ 389, L55  
 Kuijken K., Fisher D., & Merrifield M. R. 1996, MNRAS 283, 543  
 Merrifield M. R., & Kuijken K. 1994, ApJ 432, 575  
 Peale S. 1976, ARAA 14, 215  
 Quinn T. 1991, in *Warped Disks and Inclined Rings around Galaxies*, ed. S. Casertano, P. D. Sackett and F. H. Briggs (Cambridge: Cambridge University Press), 143  
 Rix H.-W., Franx M., Fisher D., & Illingworth G. 1992, ApJ 400, L5  
 Rubin V. C., Graham J. A., & Kenney J.D.P. 1992, ApJ 394, L9  
 Sellwood J. A., & Merritt D. 1994, ApJ 425, 530  
 Sridhar S., & Touma J. 1996, MNRAS 279, 1263  
 Steiman-Cameron T., & Durisen, R. H. 1984, ApJ 276, 101  
 Thakar A. R., & Ryden, B. S. 1998, ApJ 506, 93  
 Thomas P. A., Vine S., & Pearce F. R. 1994, MNRAS 268, 253  
 Tremaine S., & Weinberg M. D. 1984, MNRAS 209, 729  
 van Albada T. S., Kotanyi C. G., & Schwarzschild M. 1982, MNRAS 198, 303  
 Varnas S. R. 1990, MNRAS 247, 674  
 Whitmore B. C., et al. 1990, AJ 100, 1489

<sup>†</sup> Numerical simulations of polar rings (Habe & Ikeuchi 1985; Varnas 1990; Quinn 1991; Katz & Rix 1992; Christodoulou et al. 1992; Bekki 1998) show that gas rings on the long-axis loop orbits in triaxial potentials can be stable in the presence of dissipation, even though the libration zone surrounds a local maximum of the averaged Hamiltonian (13).